Functional Interaction of Ca_V Channel Isoforms with Ryanodine Receptors Studied in Dysgenic Myotubes

Ralph Peter Schuhmeier,* Elodie Gouadon,* Daniel Ursu,* Nicole Kasielke,[†] Bernhard E. Flucher,[†] Manfred Grabner,[‡] and Werner Melzer*

*Department of Applied Physiology, University of Ulm, Ulm, Germany; [†]Department of Physiology and Medical Physics, and [‡]Department of Medical Genetics, Molecular and Clinical Pharmacology, Innsbruck Medical University, Innsbruck, Austria

ABSTRACT   The L-type Ca^{2+} channels $Ca_V1.1$ (α_{1S}) and $Ca_V1.2$ (α_{1C}) share properties of targeting but differ by their mode of coupling to ryanodine receptors in muscle cells. The brain isoform $Ca_V2.1$ (α_{1A}) lacks ryanodine receptor targeting. We studied these three isoforms in myotubes of the α_{1S}-deficient skeletal muscle cell line GLT under voltage-clamp conditions and estimated the flux of Ca^{2+} (Ca^{2+} input flux) resulting from Ca^{2+} entry and release. Surprisingly, amplitude and kinetics of the input flux were similar for α_{1C} and α_{1A} despite a previously reported strong difference in responsiveness to extracellular stimulation. The kinetic flux characteristics of α_{1C} and α_{1A} resembled those in α_{1S}-expressing cells but the contribution of Ca^{2+} entry was much larger. α_{1C} but not α_{1A}-expressing cells revealed a distinct transient flux component sensitive to sarcoplasmic reticulum depletion by 30 μM cyclopiazonic acid and 10 mM caffeine. This component likely results from synchronized Ca^{2+}-induced Ca^{2+} release that is absent in α_{1A}-expressing myotubes. In cells expressing an α_{1A}-derivative ($\alpha_1Aas(1592$-clip)) containing the putative targeting sequence of α_{1S}, a similar transient component was noticeable. Yet, it was considerably smaller than in α_{1C}, indicating that the local Ca^{2+} entry produced by the chimera is less effective in triggering Ca^{2+} release despite similar global Ca^{2+} inward current density.

INTRODUCTION

The mobilization of Ca^{2+} for force activation in muscle cells involves the rapid communication of voltage-dependent Ca^{2+} channels with the ryanodine receptors of the sarcoplasmic reticulum (SR) (Rüegg, 1986; Melzer et al., 1995; Bers, 2001; Dirksen, 2002; Beam and Horrowitz, 2004). In cardiac cells, a Ca^{2+} inward flux mediated by voltage-operated L-type Ca^{2+} channels triggers a larger secondary Ca^{2+} efflux from the SR (DelPrincipe et al., 1999; Cheng and Wang, 2002). This mechanism requires the close proximity of the pore-forming subunit α_{1C} of the cardiac L-type channel ($Ca_V1.2$) with the Ca^{2+} release channel of the SR (ryanodine receptor RyR2) (Franzini-Armstrong et al., 1999; Bers, 2001). In contrast, the skeletal muscle L-type Ca^{2+} channel ($\alpha_{1S} = Ca_V1.1$) interacts with the ryanodine receptor (RyR1) via a direct physical link (Dirksen, 2002; Beam and Horrowitz, 2004). The protein-protein interaction is reflected in a regular tetrameric pattern (junctional tetrads) formed by the $Ca_v1.1$ in the transverse tubular (TT) membrane opposite the RyR1 clusters (Franzini-Armstrong et al., 1998, 2004). The correct targeting to the TT-SR junction that is essential for both types of interaction mechanisms seems to depend on amino acid sequences in the C-terminal regions of α_{1C} and α_{1S} (Flucher et al., 2000; Proenza et al., 2000). The skeletal muscle-specific type of direct interaction with the ryanodine receptor, on the other hand, has been attributed to specific sequences in the II–III loop of the α_{1S} isoform (Nakai et al., 1998; Grabner et al., 1999; Dirksen, 2002) and may involve further cytoplasmic regions of this protein (Ahern et al., 2001) as well as the participation of the auxiliary β_{1a} subunit (Beurg et al., 1999a,b).

The α_{1A}-subunit ($Ca_V2.1$) of neuronal P/Q-type Ca^{2+} channels is thought to lack both a specific junctional targeting sequence as well as a RyR interaction domain (Flucher et al., 2000). Immunolabeling after heterologous expression in α_{1S}-deficient dysgenic myotubes showed colocalization with RyR1 for α_{1S} and α_{1C} but not for α_{1A}. However, a chimeric construct consisting of a truncated form of α_{1A} fused with the distal half of the C-terminal α_{1S} sequence, $\alpha_1Aas(1592$-clip), restored targeting to the ryanodine receptor based on the immunostaining results (Flucher et al., 2000).

The scheme of Fig. 1 summarizes putative functional properties of the four α_1 variants in dysgenic myotubes: All constructs except α_{1S} should lead to intracellular Ca^{2+} signals that depend on the size of the voltage-activated Ca^{2+} inward current rather than on membrane voltage alone. Because of the lack of specific junctional targeting, α_{1A} should be least effective in triggering secondary Ca^{2+} release and may even not be able to cause Ca^{2+} release at all. Finally, $\alpha_1Aas(1592$-clip), like α_{1C}, would be expected to restore cardiac-type EC coupling exhibiting a significant secondary Ca^{2+} release component.

The functional data presently available can be summarized as follows: Only for α_{1S}, Ca^{2+} transients were relatively independent of the Ca^{2+} inward current (García et al., 1994; Flucher et al., 2000), consistent with the particular type of
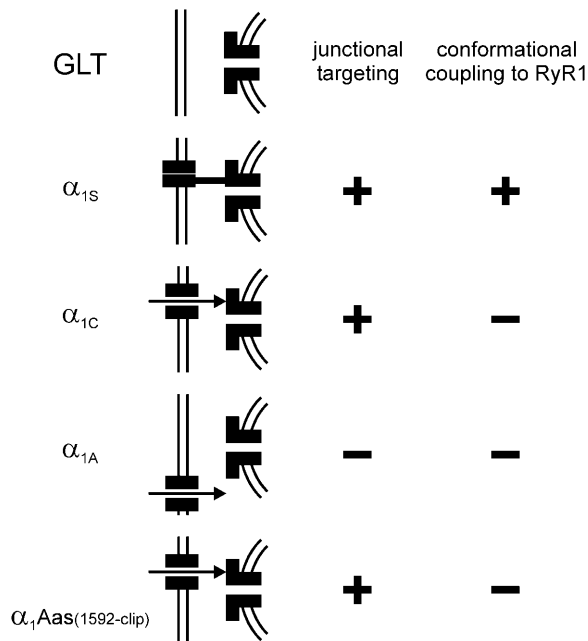
FIGURE 1   Expression of different Ca^{2+} channel α_1-subunits in dysgenic (*GLT*) myotubes. The four Ca^{2+} channel α_1-subunits that were expressed in the α_1-deficient GLT myotubes are known to differ in their location (specific targeting to the TT-SR junction or not) and their mode of interaction with the ryanodine receptor (direct mechanical coupling or not). Based on previous structural and functional investigations, α_{1S} controls release from the SR without the participation of a Ca^{2+} inward flux. α_{1C} and α_1Aas(1592-clip) which are colocalized with RyR1 should support Ca^{2+} inward current-induced Ca^{2+} release whereas α_{1A} which was reported not to be targeted to the junction should not be able to functionally interact with the junctional ryanodine receptors.

coupling mechanism. Compared with α_{1C}-expressing dysgenic myotubes, α_{1A}-expressing myotubes showed considerably lower contractile activity when subjected to extracellular electrical stimulation (Adams et al., 1994; Grabner et al., 1998). This was attributed to the lack of junctional targeting of α_{1A} (Flucher et al., 2000). The expression of the chimera α_1Aas(1592-clip), which exhibited junctional targeting (Flucher et al., 2000), produced larger Ca^{2+} current densities than α_{1A} and more frequently intracellular Ca^{2+} transients in response to extracellular stimulation. On the other hand, α_1Aas(1592-clip) showed considerably lower responsiveness than α_{1S} and α_{1C} under these conditions: the number of myotubes responding with a Ca^{2+} transient per investigated culture dish increased in the order $\alpha_{1A} < \alpha_1$Aas(1592-clip) $< \alpha_{1S} < \alpha_{1C}$ with relative values of 1, 9, 133, and 140 (Flucher et al., 2000). Because the resting potential and the shape of the action potential may vary with the type of Ca^{2+} channel expressed, the different responsiveness might also result from differences in the excitation process. We therefore investigated myotubes of the dysgenic cell line GLT (Powell et al., 1996) expressing these four Ca^{2+} channel isoforms (Fig. 1) under identical voltage-clamp conditions. In a search for differences in their

gating properties, we simultaneously measured transmembrane Ca^{2+} inward currents and intracellular Ca^{2+} signals to determine their time course and voltage-dependence. For skeletal and cardiac cells, methods have been developed to estimate the flux of Ca^{2+} mobilization (termed Ca^{2+} input flux, i.e., the sum of Ca^{2+} release flux from the SR and Ca^{2+} entry flux from the extracellular space) from optical recordings of Ca^{2+} transients (for references, see Bers, 2001; Schuhmeier and Melzer, 2004). Here, we applied this approach for the first time to transfected cells. We estimated the gain of EC coupling, i.e., the ratio of Ca^{2+} input to Ca^{2+} entry flux during step depolarization (for references, see Bers, 2001; Cheng and Wang, 2002). We further depleted the SR to estimate the relative contributions of Ca^{2+} release and Ca^{2+} entry flux to the measured Ca^{2+} signals.

MATERIALS AND METHODS

Solutions and media

The following solutions were used in the cell culture:

> Growth medium—Dulbecco's Modified Eagle Medium (DMEM) with 1% glutamine (200 mM), 10% fetal calf serum (FCS), and 10% horse serum (HS).
> Trypsin solution—Trypsin-EDTA (0.05–0.53 μM) in Ca^{2+}- and Mg^{2+}-free phosphate-buffered saline (PBS).
> Fusion medium—DMEM with 1% glutamine (200 mM) and 2% HS.
> Transfection medium—100 μl per 35-mm dish, containing 94 μl serum-free DMEM, 6 μl Fugene 6 (see below), and 2 μg DNA.

The experimental recording solutions had the following compositions:

> External solution—130 mM tetraethylammonium hydroxide, 127 mM HCl, 10 mM $CaCl_2$, 1 mM $MgCl_2$, 2.5 mM 4-aminopyridine, 0.00125 mM tetrodotoxin, and 10 mM HEPES, pH-adjusted to 7.4 with HCl.
> Internal (pipette) solution—145 mM CsOH, 145 mM aspartic acid, 0.1 mM EGTA, 0.01 mM $CaCl_2$ (free Ca^{2+}, 10^{-5} mM), 1.14 mM Na_2ATP, 3.86 mM MgATP (Mg/ATP ratio according to supplier, 1.4; free Mg^{2+}, 1 mM), 5 mM Na creatine phosphate, 0.2 mM K_5-Fura-2, and 10 mM HEPES, pH-adjusted to 7.4 with CsOH.

DMEM, HS, and Trypsin-EDTA were purchased from Gibco (Karlsruhe, Germany), FCS, and PBS from PAA Laboratories (Cölbe, Germany), rat tail collagen (Typ 1, C 7661), EGTA, ATP, caffeine, cyclopiazonic acid, and CsOH from Sigma-Aldrich (Taufkirchen, Germany), Fugene 6 from Roche Biochemicals (Mannheim, Germany), TEA and HEPES from Merck (Darmstadt, Germany), tetrodotoxin and Fura-2 from Molecular Probes (Leiden, Netherlands), creatine phosphate from Boehringer (Mannheim, Germany), 4-aminopyridine from Fluka (Neu-Ulm, Germany), and L-glutamine from Biochrom (Berlin, Germany).

Cell culture and transfection

For heterologous expression of the Ca^{2+} channel α_1-subunits, we used myotubes of the homozygous dysgenic (mdg/mdg) cell line GLT that was originally generated by transfection of mdg myoblasts with a plasmid-encoding Large-T Antigen (Powell et al., 1996). GLT myoblasts were expanded in growth medium at 10% CO_2 and 37°C and passaged before reaching 80% confluence using trypsin detachment. To obtain myotubes,

cells were plated onto carbon- and gelatin-coated coverslips in 35-mm dishes. After reaching confluence, growth medium was exchanged for fusion medium. We used mammalian expression plasmids coding for N-terminally GFP-tagged fusion proteins of the Ca^{2+} channel pore-forming subunits α_{1S}, α_{1C}, α_{1A}, and α_{1A}as(1592-clip), respectively, as described by Flucher et al. (2000). Cells were transfected at the onset of fusion. Measurements were made from the myotubes four days later.

Electrophysiology and fluorimetry

Whole-cell patch-clamp experiments and microfluorimetric recordings were performed at room temperature (20–23°C) as described by Schuhmeier et al. (2003) and Schuhmeier and Melzer (2004). Briefly, myotubes were loaded with Fura-2 by diffusion from a patch-pipette containing internal solution (see above). Leak-resistance and capacitance were determined by using small positive and negative pulse excursions (10 mV amplitude, 25 ms duration) from the holding potential. Linear leak correction of current recordings was performed by a standard p/n method ($n = 4$ or 8). Ca^{2+}-dependent fluorescence changes were recorded at 515 nm while exciting at 380 nm (F_{380}). After background correction, the F_{380} recordings were normalized either by F_{380} measurements preceding each voltage-clamp activation (Figs. 2–4, displayed as $-\Delta F/F_0$), or by F_{360} (Figs. 5–8), as described in Schuhmeier et al. (2003).

Data analysis

General analysis and nonlinear curve fitting were carried out using Excel (MicroSoft, Seattle, WA) and Origin (OriginLab, Northampton, MA). The program CalcV22 (Föhr et al., 1993) was used to calculate the free ion concentrations in the internal solution.

The leak-corrected ionic currents $I(V)$ were normalized by the linear capacitance to obtain current densities $i(V)$. The voltage-dependence of the Ca^{2+} current density $i_{Ca}(V)$ was least-squares-fitted with Eq. 1:

$$i_{Ca}(V) = f(V) g_{Ca,max}(V - V_{Ca}), \tag{1}$$

$$f(V) = \frac{1}{1 + \exp((V_{0.5} - V)/k)}. \tag{2}$$

The values $g_{Ca,max}$ and V_{Ca} are maximal normalized conductance and reversal potential, respectively, of the L-type Ca^{2+} current; $f(V)$, voltage-dependence of activation; and $V_{0.5}$ and k, voltage of half-maximal activation and voltage sensitivity parameter, respectively. The fit also included correction for a small offset resulting from noise effects in the minimum detection.

Ca^{2+} current densities i_{Ca} were converted to Ca^{2+} entry flux using Eq. 3:

$$\frac{d}{dt}[Ca^{2+}]_{i_{Ca}} = \frac{i_{Ca}}{zFf_V V_C}. \tag{3}$$

Here, z is the valence of the Ca^{2+} ion, F is the Faraday's constant, V_C is the intracellular volume per membrane capacitance, and f_V is the fraction of the total volume that is immediately accessible to Ca^{2+}.

Free Ca^{2+} concentration was determined using background- and bleaching-corrected fluorescence ratio signals ($R = F_{380}/F_{360}$) according to Eq. 4 (Klein et al., 1988):

$$[Ca^{2+}] = K_{D,Fura} \left[\frac{\dfrac{1}{k_{off,Fura}} \times \dfrac{dR}{dt} + R - R_{min}}{R_{max} - R} \right]. \tag{4}$$

The following values were used for R_{min} (fluorescence ratio at zero dye saturation), R_{max} (ratio at full dye saturation), and $K_{D,Fura}$ (dissociation
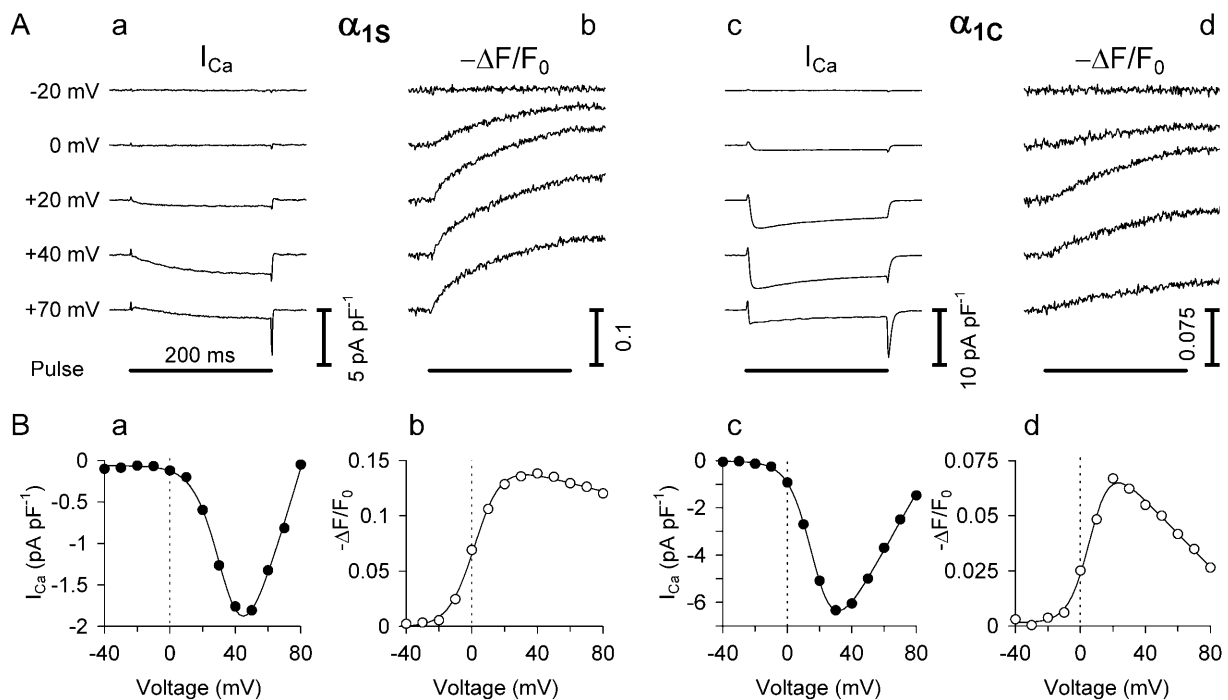

FIGURE 2   Simultaneously recorded Ca^{2+} inward currents and intracellular Ca^{2+} signals in GLT myotubes. (A) Recordings of leak-corrected Ca^{2+} inward currents (a and c) and fluorescence changes (b and d) in GLT myotubes transfected with expression plasmids carrying cDNA encoding α_{1S} and α_{1C}, respectively. (B) Peak Ca^{2+} current densities (a and c) and Ca^{2+} transients (b and d) as functions of voltage. Continuous lines are least-squares fits with Eqs. 1 and 2, i.e., formally the same functions were used to describe the voltage-dependence of transmembrane Ca^{2+} current density and intracellular Ca^{2+} transient.

constant of the dye): 2.84, 0.68, and 276 nM, respectively (see Schuhmeier et al., 2003). For the Fura-2 dissociation rate constant $k_{\text{off,Fura}}$ we used the value of 46.4 s^{-1} (Schuhmeier and Melzer, 2004).

An estimate of the flux of Ca^{2+} mobilization in the myoplasm (called *Ca^{2+} input flux*) during strong depolarizations was calculated with a Ca^{2+} binding model using the general method of Baylor et al. (1983). The free Ca^{2+} transient (Eq. 4), averaged for three sequential voltage pulses (+30 mV) of 100-ms duration, applied at 30-s intervals, was used to calculate the Ca^{2+} occupancies of the model components. Free Ca^{2+} and the estimated occupancies were summed and the time derivative calculated. Differential equations were solved using Euler's method. The calculation employed a digital filter that adjusted its bandwidth automatically to the signal dynamics (Schuhmeier et al., 2003). In the model we used troponin C with concentration (120 μM) and kinetic properties as reported for skeletal muscle fibers (Baylor and Hollingworth, 1998). Each molecule of troponin C has two fast, Ca^{2+}-specific binding sites (*T-sites*) and two slow Ca^{2+}-Mg^{2+}-binding sites (*P-sites*) with rate constants $k_{\text{on,T,Ca}} = 88.5\ \mu$M^{-1} s^{-1}, $k_{\text{off,T,Ca}} = 115$ s^{-1}, $k_{\text{on,P,Ca}} = 41.7\ \mu$M^{-1} s^{-1}, $k_{\text{off,P,Ca}} = 0.5$ s^{-1}, $k_{\text{on,P,Mg}} = 0.033\ \mu$M^{-1} s^{-1}, and $k_{\text{off,P,Mg}} = 3$ s^{-1}. In contrast to mature muscle fibers, there is no evidence for the presence of parvalbumin in developing muscle (Leberer and Pette, 1986). EGTA (0.1 mM) in the myoplasm was described by using the means of in situ rate constants ($k_{\text{on,S}} = 20\ \mu$M^{-1} s^{-1} and $k_{\text{off,S}} = 2.71$ s^{-1}) determined empirically in C2C12 myotubes loaded with large excess of EGTA (Schuhmeier and Melzer, 2004). Because SR uptake rates in myotubes seem to be small compared to release rates during depolarization (García and Beam, 1994), a component simulating the SERCA pump was not included in the model.

Statistics

Data are presented as *means ± SE* (*n = number of experiments*) for averaged values, and as *parameter ± SE* for best-fit parameters.

RESULTS

To determine the voltage-dependence of both Ca^{2+} inward currents and Ca^{2+} transients, the pulse paradigm described in Fig. 2 was used. The recordings in Fig. 2 *A* were obtained from one GLT cell expressing α_{1S} (*a* and *b*) and another one expressing α_{1C} (*c* and *d*). The length of the voltage-clamp pulse was 200 ms in all cases (*horizontal bar*). Leak-corrected Ca^{2+} inward current (I_{Ca}) and normalized change in fluorescence ($-\Delta F/F_0$) are displayed next to each other for a series of pulses from -20 mV to $+70$ mV.

Fig. 2 *B* depicts the voltage-dependence obtained from each series of recordings, upon taking the signal peak for the inward current (*solid symbols*) and the average of the last 10 ms during the pulse for the fluorescence (*open symbols*). Clearly, in the case of α_{1S} the threshold for activation of Ca^{2+} transients (*b*) is considerably more negative than for the activation of inward current (*a*) and Ca^{2+} transients are of almost equal amplitude between $+50$ and $+80$ mV. In contrast, in the case of α_{1C}, Ca^{2+} current (*c*) and Ca^{2+} transient (*d*) start at a similar potential and show a similar decline in amplitude at large depolarizing potentials.

Fig. 3 compares voltage-dependence of Ca^{2+} current (*solid symbols*) and Ca^{2+} transient (*open symbols*) for each of the α_1-subunit types of Fig. 1 using averaged data of individual experiments. α_{1S} produced the smallest Ca^{2+}
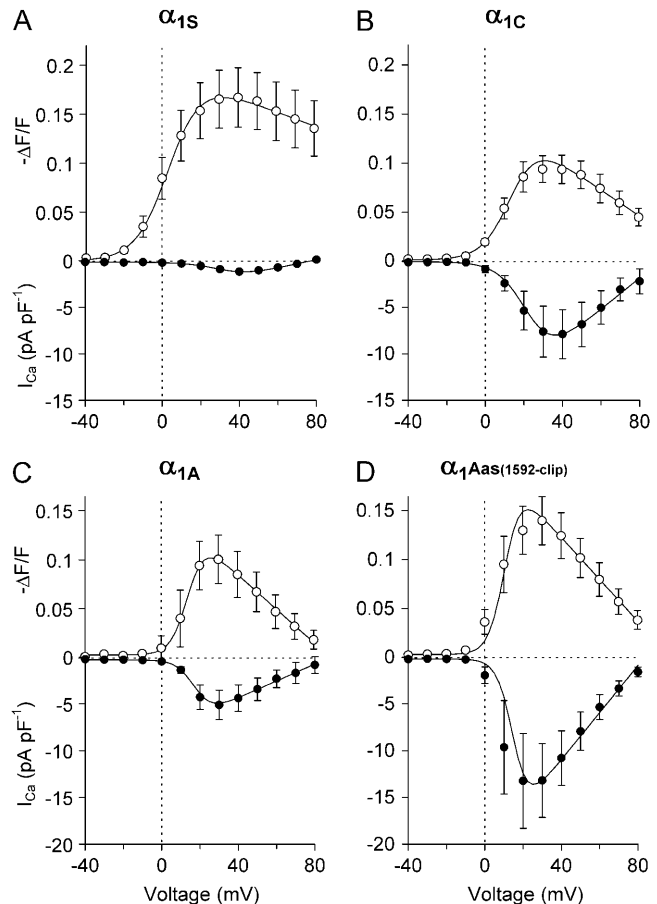

FIGURE 3 Voltage-dependence of Ca^{2+} inward current density and intracellular Ca^{2+} transient. Mean data obtained from recordings in transfected GLT myotubes. (*A*) α_{1S} (*n = 6*), (*B*) α_{1C} (*n = 5*), (*C*) α_{1A} (*n = 5*), and (*D*) α_1Aas(1592-clip) (*n = 10*). The continuous curves show least-squares fits according to Eqs. 1 and 2 (see also Fig. 2).

current densities but the largest Ca^{2+} transients (Fig. 3 *A*). The α_{1S}-transients show only a small decrease in amplitude at large voltages whereas the decrease is substantial in the three other cases (Fig. 3, *B–D*). The bell-shaped fluorescence-voltage relations for α_{1C}, α_{1A}, and α_1Aas(1592-clip) indicate a close relation between inward current and Ca^{2+} signal. The maximal mean Ca^{2+} signal of α_{1S} was significantly larger than that of α_{1C} and α_{1A} (but not α_1Aas(1592-clip)). The putative junctionally targeted α_1Aas(1592-clip) showed a significantly larger maximal current density than the nontargeted α_{1A} channel. On the other hand, the amplitude of the α_1Aas(1592-clip) Ca^{2+} signal was not found to be significantly larger than that of α_{1A}.

To better compare the voltage-dependence of activation of Ca^{2+} current and intracellular Ca^{2+} transients we formally fitted both leak-corrected current and fluorescence data in Fig. 3 with Eq. 1. The best-fit functions are superimposed on the data points as continuous lines using the means of the individual best-fit parameters.
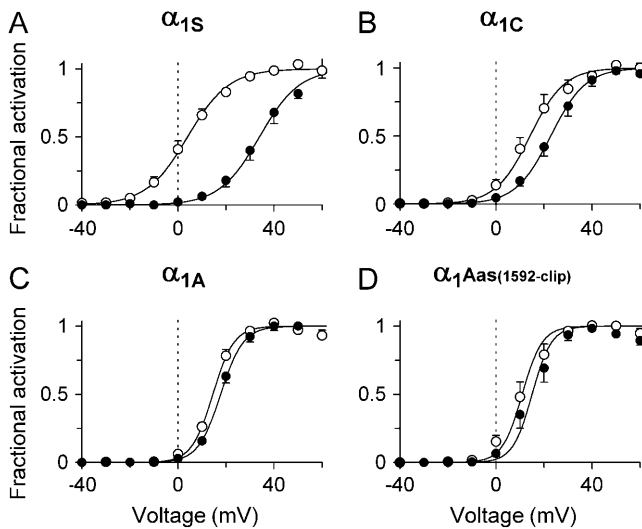
FIGURE 4 Voltage-dependence of activation. The inward current data of Fig. 3 were converted to fractional conductance using Eq. 1 and solving for $f(V)$ (*solid symbols*). A formally equivalent conversion was performed using the optically recorded Ca^{2+} signal data of Fig. 3 (*open symbols*). The two types of activation curves differ clearly for α_{1S} (A) and to a lesser degree for α_{1C} (B), whereas for α_{1A} (C) and α_1Aas(1592-clip) (D), the difference is below 5 mV.

Fig. 4 displays the data of Fig. 3 after conversion to $f(V)$ to show the voltage-dependence of fractional activation according to Eq. 2. If the Ca^{2+} transient is the immediate result of the Ca^{2+} entry flux, the two activation curves are expected to be similar. As can be seen from these plots, for the skeletal muscle α_1-subunit (α_{1S}), the optically recorded Ca^{2+} transient reaches its half-maximal value at a considerably more negative potential than the Ca^{2+} conductance activation (Fig. 4 A, *open* and *solid circles*, respectively). The midpoint voltages of activation are separated by 29.9 mV. In the case of the cardiac α_1-subunit (α_{1C}) the activation curves are closer together, but still separated by a gap of $\sim$8.6 mV (Fig. 4 B). In contrast, the two activation curves show much smaller differences for α_{1A} and its chimeric construct, 3.3 and 4.1 mV, respectively (Fig. 4, C and D).

Table 1 summarizes the parameters describing the voltage-dependence obtained from the data of Figs. 3 and 4. The two L-type channels can be easily distinguished from α_{1A} and its

chimeric derivative by the lower steepness of activation (larger k). Within each group, steepness of activation of Ca^{2+} entry and intracellular Ca^{2+} signals were similar.

Estimating voltage-dependent Ca^{2+} fluxes

The different modes of EC coupling and different targeting properties of the four types of channels (Fig. 1) might result in detectable differences in kinetic features of the SR Ca^{2+} release flux. Therefore, we converted fluorescence ratio signals measured in a further set of experiments to estimates of the total flux of Ca^{2+} into the myoplasmic water space (Ca^{2+} input flux), i.e., the sum of the two voltage-activated flux components (Ca^{2+} entry and Ca^{2+} release) underlying the recorded Ca^{2+} transients. To obtain sufficiently high signal/noise ratios we performed these experiments at a voltage close to the maximum of inward current and Ca^{2+} transient amplitude. Three pulses of 100-ms duration depolarizing the membrane to +30 mV were applied at 30-s intervals and the recorded signals were averaged. To calculate the dynamics of intracellular Ca^{2+} binding and to estimate the Ca^{2+} input flux from the optical measurements, we used a model-based approach similar to that originally described by Baylor et al. (1983) and previously used for skeletal myotubes (Dietze et al., 1998, 2000; Ursu et al., 2001; Schuhmeier et al., 2003). A set of kinetic constants describing the intracellular binding sites that likely predominate under our conditions was taken from the literature and from our own experimental results obtained in C2C12 myotubes, and was used for the model calculations (Schuhmeier and Melzer, 2004; for more details, see Materials and Methods).

In some experiments with α_{1S}-expressing myotubes, we also applied the approach described recently to determine Ca^{2+} input flux in C2C12 myotubes equilibrated with a high concentration (15 mM) of EGTA in the pipette solution (Schuhmeier and Melzer, 2004). In this method, removal model parameters were determined by a least-squares fitting of model-calculated to measured Ca^{2+} transients in the time intervals after depolarizing pulses. This method was not generally used in the present investigation, because of low signal/noise ratios that made the numerical calculations

TABLE 1 Parameters of voltage-dependent activation of Ca^{2+} inward currents and intracellular Ca^{2+} transients

	Ca^{2+} current				Ca^{2+} transient			
	α_{1S}	α_{1C}	α_{1A}	α_1Aas (1592-clip)	α_{1S}	α_{1C}	α_{1A}	α_1Aas (1592-clip)
$V_{0.5}$ (mV)	33.9 ± 2.7	22.8 ± 2.5	17.8 ± 0.9	15.0 ± 2.5	4.0 ± 2.1	14.2 ± 3.4	14.5 ± 0.9	10.9 ± 2.5
k (mV)	8.3 ± 0.4	7.3 ± 0.3	4.7 ± 0.5	4.1 ± 0.3	8.6 ± 0.2	7.2 ± 0.6	4.4 ± 0.3	4.2 ± 0.1
$g_{Ca.max}$ (pS/pF)	45 ± 5	169 ± 40	90 ± 21	252 ± 76				
V_{Ca} (mV)	74.6 ± 3.5	87.8 ± 4.8	80.6 ± 12.0	84.9 ± 4.3				
n	6	5	5	10	6	5	5	10

Current-voltage relations and fractional changes in the fluorescence ratio signals were fitted with Eqs. 1 and 2 as described in Materials and Methods. n = number of cells.

difficult and because of possible suppression of Ca^{2+}-induced Ca^{2+} release by the strong EGTA buffering. Two α_{1S}-expressing cells that were analyzed in this way showed removal parameter results and a time course of Ca^{2+} input flux comparable to those determined in C2C12 cells (Schuhmeier and Melzer, 2004). They also showed a pha-sic-tonic time course similar to that estimated for the α_{1S}-expressing cells in the present experiments with 0.1 mM EGTA in the pipette solution.

In addition to the Ca^{2+} input flux derived from the optical indicator signal, the flux of Ca^{2+} entry was determined from the electrically measured Ca^{2+} inward current. The trans-membrane Ca^{2+} inward current density was converted to flux according to Eq. 3. The necessary volume/capacitance ratios (V_C) were measured by scanning dye-loaded and whole-cell patch-clamped GLT myotubes with a confocal microscope as described by Schuhmeier et al. (2003). Volume (corrected for the space occupied by nuclei) was approximately proportional to capacitance in the range 200–800 pF, with a best-fit proportionality factor of $V_C = 0.26\ l/F$ that was used for the calculation. The factor f_V was arbitrarily set to 1 (the upper bound of this value).

Fig. 5 A shows the averaged Ca^{2+} input flux records obtained at $+30$ mV in a number of cells expressing the four different α_1-subunits shown in Fig. 1. Mean values are displayed as thick lines and their standard errors as shaded areas. The corresponding Ca^{2+} entry flux traces derived from the Ca^{2+} inward currents are plotted in Fig. 5 B with the same scale (for comparison of flux amplitudes) but opposite in sign.

Even though the calculated *absolute* flux amplitudes are somewhat questionable because of uncertainties in the model parameters, a relative comparison shows some interesting details. Consistent with Fig. 3, the Ca^{2+} input flux was found to be largest in the α_{1S}-expressing myotubes whereas the Ca^{2+} entry flux was very small, indicating that essentially all the Ca^{2+} input flux resulted from SR Ca^{2+}
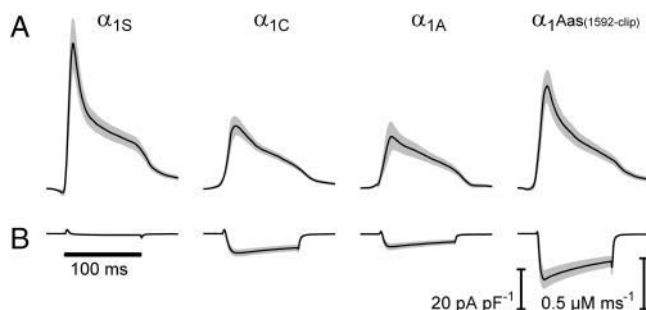
release. α_1Aas(1592-clip), the brain α_1-subunit carrying the putative signal sequence for SR-TT junctional targeting, showed the second-largest flux amplitude. Here, however, the Ca^{2+} entry flux from the extracellular space was many times larger than in the case of α_{1S}. Therefore, a much larger part of the total estimated Ca^{2+} input flux resulted from Ca^{2+} entry and it appears difficult to determine which component of the Ca^{2+} input flux results from SR Ca^{2+} release and which from Ca^{2+} entry. A similar situation exists for α_{1A} and α_{1C}.

Based on previous physiological data, one should expect clear differences between the junctionally targeted and nontargeted channels in their effectiveness to elicit in-tracellular Ca^{2+} transients. When activated by extracellular electrical stimulation, α_{1A}-expressing myotubes had been reported to show much weaker force and Ca^{2+} responses than α_{1C}-expressing myotubes which was attributed to the lack of specific junctional targeting (Flucher et al., 2000). In contrast to this, under voltage-clamp conditions in the present experiments, both channel types produced approx-imately equal input flux amplitudes.

Estimating EC coupling gain

The ratio of Ca^{2+} transient amplitude to Ca^{2+} inward current has frequently been used as a measure of EC coupling gain (for references, see Bers, 2001). On the other hand, the ratio between total Ca^{2+} input flux, which includes Ca^{2+} release, and the flux of Ca^{2+} entry, defines a physically more meaningful gain (Wier et al., 1994). Using the flux deter-minations of Fig. 5, we determined average EC coupling gain factors by calculating the mean ratio between total Ca^{2+} input flux and Ca^{2+} entry flux in a broad time interval during the pulse (from 25 ms to 75 ms) excluding the rapid phases of activation and deactivation. If the absolute amplitudes of the fluxes were correctly determined, a value of 1 of the gain factor would mean that no secondary release of Ca^{2+} from intracellular stores is present, i.e., all measured Ca^{2+} changes result from Ca^{2+} entering from the extracellular space. For the α_{1S}-subunit, this gain factor was many times >1 (mean value 31.5 ± 4.4), consistent with the major contribution of the SR Ca^{2+} release to the Ca^{2+} transient and the negligible role of the Ca^{2+} current. For the three subunits that show no skeletal-type conformational coupling, the ratios were 3.2 ± 0.5 (α_{1C}), 3.9 ± 0.4 (α_{1A}), and 2.0 ± 0.3 (α_1Aas(1592-clip)). That is, quite consistent with the experiments of Fig. 3, there were no large differences between the three non-skeletal-type chan-nels in their mean EC coupling gain.

Effects of SR depletion

These results indicate that Ca^{2+} entry makes a substantial contribution to the total Ca^{2+} input flux, with the exception of α_{1S}. However, considering the uncertainties in determin-ing the absolute flux amplitudes (see above), it seems

FIGURE 5 Comparison of Ca^{2+} input flux and Ca^{2+} entry flux. (A) Averaged Ca^{2+} input flux calculations for the constructs shown in Fig. 1 during 100 ms depolarizations to $+30$ mV. (B) Averaged Ca^{2+} inward current densities for the same pulses that elicited the records in A. Number of experiments from left to right: $n = 17, 16, 16,$ and 15. Thick lines indicate mean values; shaded areas indicate mean $\pm$ SE.

difficult to quantify the true fractional contribution. In particular, the value larger than unity for the gain factor of the non-junctionally targeted α_{1A}-subunit may result from a Ca^{2+} release component in addition to Ca^{2+} entry or from false assumptions in the calculation of the absolute flux amplitudes leading to overestimation of Ca^{2+} input flux, underestimation of Ca^{2+} entry flux, or both. We therefore performed experiments in which the SR was depleted of its stored Ca^{2+} by applying 30 μM cyclopiazonic acid (CPA), a blocker of the SERCA Ca^{2+} pump (Schuhmeier and Melzer, 2004), and 10 mM of the ryanodine receptor agonist caffeine (Herrmann-Frank et al., 1999). This procedure has been shown to drastically reduce the flux component resulting from SR Ca^{2+} release in C2C12 myotubes and should reveal the component that consists only of the Ca^{2+} entry through the voltage-activated Ca^{2+} channels (Schuhmeier and Melzer, 2004).

Fig. 6, A and B, demonstrates the depletion protocol. The measurements shown covered a time interval of 10 min. Application of CPA and caffeine (as indicated by the bars in Fig. 6 A) caused changes in baseline free [Ca^{2+}] values calculated from the fluorescence ratio immediately before each voltage pulse that was applied (Fig. 6 B). The mean values for each group of cells are shown. In all cases a similar increase in baseline Ca^{2+} concentration occurred when CPA was applied, indicating that a discharge of similar amounts of Ca^{2+} from the SR took place and that the loading state of the SR had not been considerably different before the application of CPA.

Fig. 6, C and D, summarize the mean results for fluxes and gains for all four α_1 isoforms. Fig. 6 C shows the means of Ca^{2+} input flux and Ca^{2+} entry flux (plotted upward and downward, respectively), obtained in the three regions labeled a, b, and c (i.e., before and after CPA application and after caffeine application). Fig. 6 D displays the means of the individually calculated gains from the data in C. The initial gains were very similar to those determined in the previous series of experiments (Fig. 5). In the α_{1S} case (left column), the input flux amplitude dropped substantially after application of CPA, whereas the entry flux (L-type current) amplitude changed only a little. Little further change was observed when applying caffeine in addition to CPA, indicating that the CPA treatment had already released most of the Ca^{2+} stored in the SR, consistent with results in
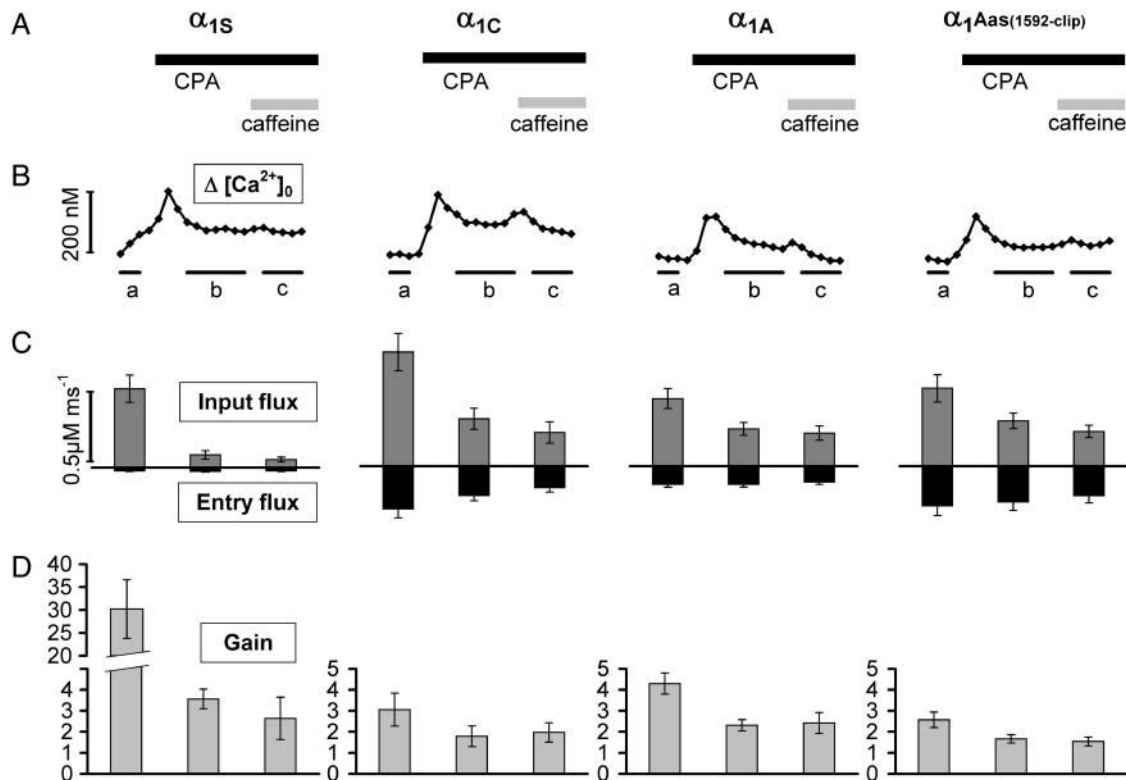

FIGURE 6 Effect of SR depletion on EC coupling gain. (A) 30 μM CPA and 10 mM caffeine were applied to deplete the SR of stored Ca^{2+} to study the effect on Ca^{2+} fluxes and gain in a number of myotubes expressing the four α_1-subunits of Fig. 1. (B) Time-dependent changes in mean baseline free Ca^{2+} concentration indicating comparable Ca^{2+} release in all cases. (C) Mean Ca^{2+} input flux and Ca^{2+} entry flux (average from 25 to 75 ms during the voltage pulse) for each of the three intervals, labeled a, before drug application; b, after CPA application; and c, after caffeine application. Entry flux plotted in opposite direction of input flux. (D) A gain factor was calculated representing the ratio of Ca^{2+} input flux (derived from the optical signals) and Ca^{2+} entry flux (derived from the inward current density) using the data of C. Because small current amplitudes produced large variances, current density amplitudes <0.5 A/F were excluded for the gain calculation of α_{1S} in D. From left to right, the numbers of cells were 7, 4, 5, and 8, respectively.

C2C12 myotubes (Schuhmeier and Melzer, 2004). In the other cases (columns *2–4*), the relative change in input flux was considerably smaller on CPA application and showed only small further changes on application of caffeine. The fractions of the initial gain that remained after CPA application showed mean values of 12%, 58%, 54%, and 65% for α_{1S}, α_{1C}, α_{1A}, and α_1Aas(1592-clip), respectively. After caffeine application the fractional values were 8.7%, 64%, 56%, and 60%, respectively.

Fig. 7 presents the mean time course of Ca^{2+} input flux and Ca^{2+} entry flux induced by the +30 mV step depolarizations averaged over the intervals *a*, *b*, and *c* indicated in Fig. 6 *B*, respectively. During depletion, Ca^{2+} input flux remained phasic (i.e., exhibits a peak) in α_{1C}, α_{1A}, and α_1Aas(1592-clip) but loses the peak in α_{1S} (see *inset*). Fig. 8 evaluates both peaks (*A*) and end level (values at 95 ms, *B*) by plotting Ca^{2+} input flux versus Ca^{2+} entry flux. The dotted lines indicate a ratio (i.e., gain) of 1. In all four cases, the gain at the pulse end approaches unity after the CPA/caffeine treatment, as would be expected for full SR depletion and a correct description of cytoplasmic Ca^{2+} binding by the model. The reason for the larger deviation

from unity gain in CPA/caffeine observed at the peak (Fig. 8 *A*) is unclear, but might be a remaining small reuptake activity of the SR that permits a transient residual Ca^{2+} release at the onset of the depolarization.

The records in Fig. 7, column 3 (*c*), represent, for each series of experiments, the maximum of depletion that could be obtained under these conditions. By subtracting this component from the record in column 1 (*a*) we calculated the fraction of the control flux that is eliminated by CPA and caffeine (Fig. 7, column 4 (*d*)). Before subtracting the *full-depletion response* (*c*), we compensated for the rundown in Ca^{2+} entry flux by multiplying entry and input flux with scaling factors to obtain equal entry flux amplitudes for each row. The depletion-sensitive component showed two phases, a rapidly and a slowly declining one. The rapidly declining phase, i.e., the peak above the dashed line in Fig. 7, column 4 (*d*), was largest in α_{1S} (*A*), intermediate in α_{1C} (*B*), and small in α_1Aas(1592-clip) (*D*). It was absent in α_{1A} (*C*). The slow component (indicated by the *dashed lines*) was similar in size for α_{1C}, α_{1A}, and α_1Aas(1592-clip), but considerably larger for α_{1S}. A tentative interpretation for these observations will be given in the Discussion in conjunction with Fig. 9.
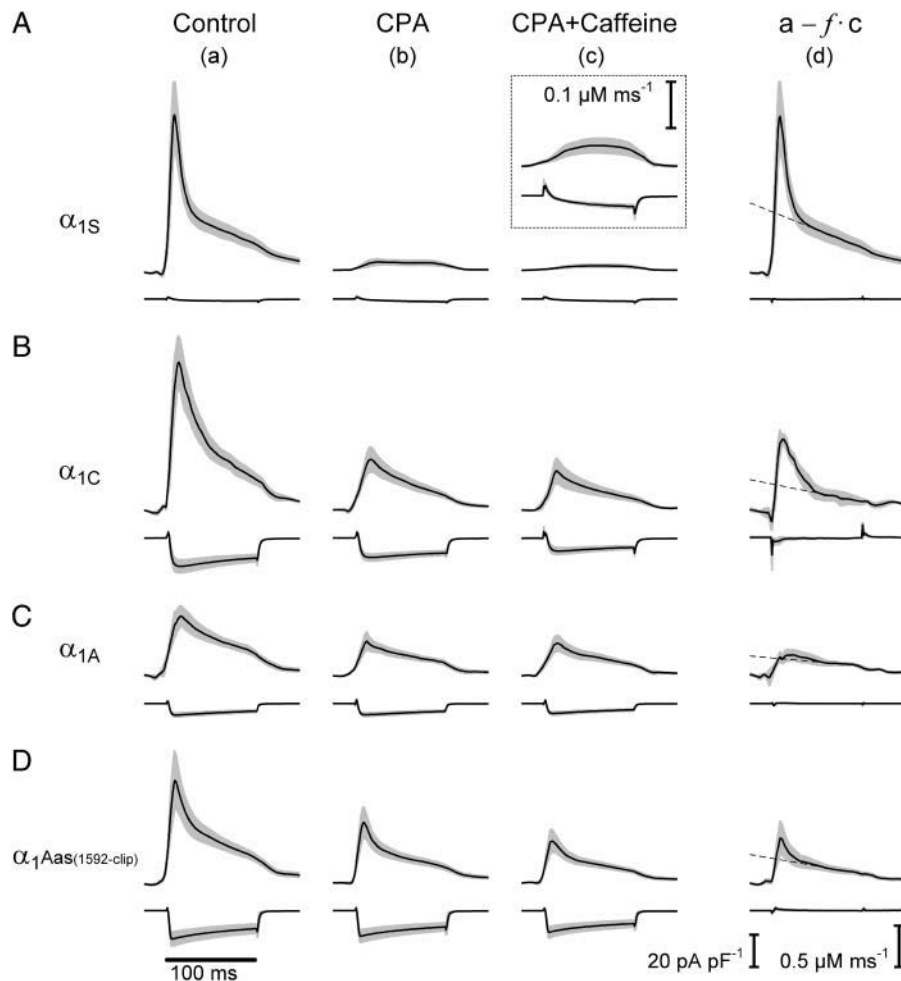

FIGURE 7 Time course of Ca^{2+} input and entry flux during SR depletion. Time course of calculated Ca^{2+} fluxes (Ca^{2+} input flux drawn upward, Ca^{2+} entry flux downward). Columns (*a*), (*b*), and (*c*) show the averaged responses to pulse depolarization (100 ms, +30 mV) in the correspondingly labeled intervals of Fig. 6 *B*, respectively. Column (*d*) shows the depletion-sensitive flux components. After scaling with a factor *f* to correct for a rundown in the current traces, the depolarization-induced responses persisting after CPA and caffeine application (column *c*) were subtracted from the responses before drug application (column *a*). The subtraction was performed for each individual experiment and the differences were averaged. Shaded areas indicate point by point SE.
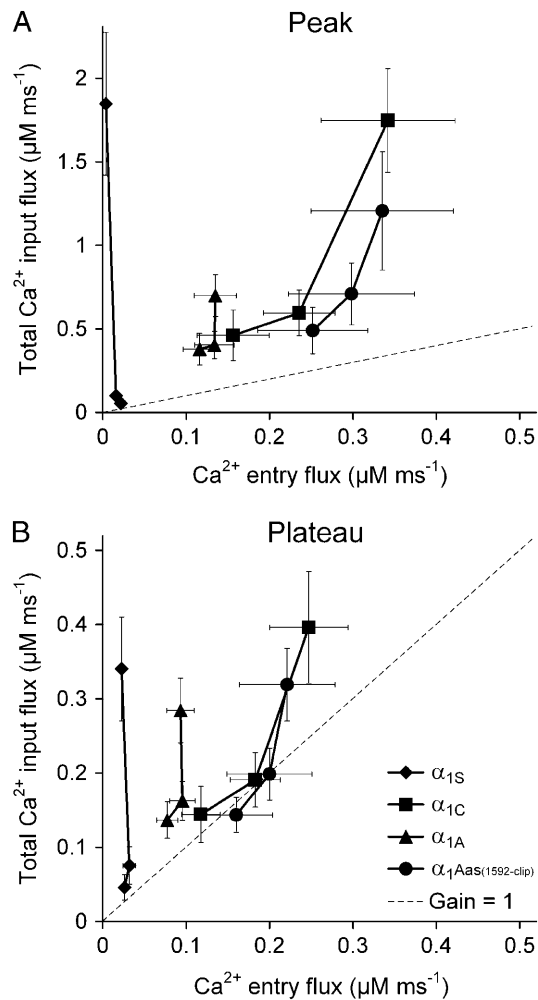
FIGURE 8 Correlation between Ca^{2+} entry flux and Ca^{2+} input flux. Mean values of Ca^{2+} input flux plotted versus corresponding means of Ca^{2+} entry flux, evaluated at the input flux peak (*A*) and near the end of the pulse (95 ms) (*B*). Each connected data points correspond to Fig. 7, *a*, *b*, and *c*.

DISCUSSION

In this study, four types of Ca$_V$-channels were expressed and investigated in dysgenic GLT myotubes (Powell et al., 1996). These channels differ in their reported cellular targeting and in their putative way of communication with the SR Ca^{2+} release channels (see Fig. 1). By studying Ca^{2+} currents and Ca^{2+} transients under voltage-clamp conditions, we identified characteristics of Ca^{2+} signaling corresponding to these differences. In contrast to previous studies on reconstituted channels in dysgenic myotubes (e.g., García et al., 1994; Jurkat-Rott et al., 1998; Ahern et al., 2001), we applied a more rigorous kinetic analysis and estimated the flux of Ca^{2+} mobilization whose time course is concealed in the Ca^{2+} transients by the kinetics of Ca^{2+} binding to the indicator dye and to intrinsic sites. Further, we quantified the gain of Ca^{2+} mobilization by determining the

ratio of the total Ca^{2+} input flux to the flux of Ca^{2+} entry from the extracellular space.

Comparison between α_{1S} and α_{1C}
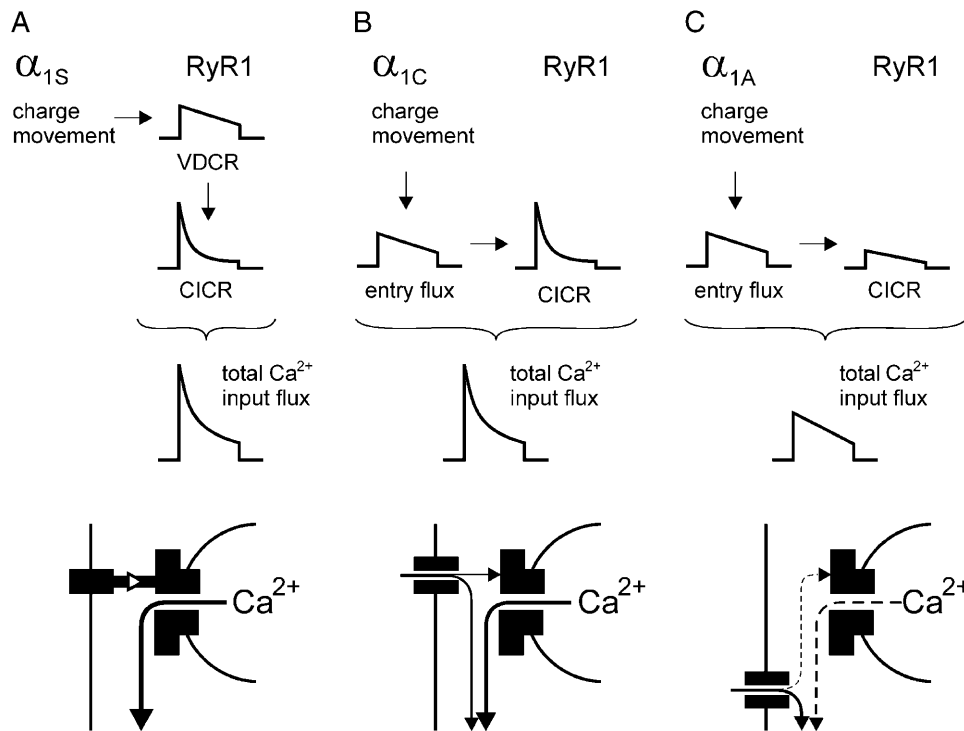
The α_{1S} channels generated Ca^{2+} input flux with a time course similar to that found in normal mammalian myotubes (Dietze et al., 1998; Ursu et al., 2001; Schuhmeier et al., 2003; Schuhmeier and Melzer, 2004) and mature muscle fibers (Delbono and Stefani, 1993; García and Schneider, 1993; Shirokova et al., 1996; Csernoch et al., 1999a,b; Ursu et al., 2004), providing evidence that the rescued Ca^{2+} release in this expression system shows the typical kinetic hallmarks of skeletal muscle type EC coupling, including the rapid partial inactivation (Melzer et al., 1984).

Despite the fundamentally different mechanisms of EC coupling in α_{1S}- and α_{1C}-expressing cells, the time courses of Ca^{2+} input flux were surprisingly similar (Fig. 7). As a major difference, depletion of the SR reduced primarily the phasic component in α_{1C}, whereas it eliminated both phasic and tonic components in α_{1S} (Fig. 7, (*d*), *B* and *A*, respectively). The reason is that the tonic component of α_{1C}-expressing cells results largely from the Ca^{2+} inward current, whereas in α_{1S}-expressing cells it is a flux from the SR, controlled by the DHPR voltage sensor (Csernoch et al., 1993). This is depicted in the idealized scheme of Fig. 9 (*A* and *B*). In both α_{1S}- and α_{1C}-expressing GLT myotubes, a pedestal flux of Ca^{2+} is activated by the membrane depolarization. Yet, in the α_{1C} case this flux component enters the myoplasm from the extracellular space (Fig. 9 *B*), whereas in the case of α_{1S} it originates from the sarcoplasmic reticulum (Fig. 9 *A*, VDCR).

Both rapid synchronous activation by conformational coupling in α_{1S}-expressing cells and rapid voltage activation of Ca^{2+} entry in α_{1C}-expressing cells likely cause similar fast primary Ca^{2+} signals in the junctional gap that probably lead to similar phasic components of CICR (Fig. 7).

Comparison between α_{1C}- and α_{1A}-controlled Ca^{2+} fluxes

Strong differences had been found between α_{1C}- and α_{1A}-expressing dysgenic myotubes in their responsiveness to extracellular electrical stimulation: Whereas α_{1C}-expressing cells responded frequently with a Ca^{2+} transient or contraction, α_{1A}-expressing cells responded only rarely (Adams et al., 1994; Flucher et al., 2000). The similar size of the fluxes obtained in the two groups of cells in our voltage-clamp experiments seemed, therefore, surprising (Fig. 5). At closer look, however, differences could be detected. The Ca^{2+} input flux component in α_{1A} cells that is sensitive to SR depletion by CPA and caffeine (Fig. 7 *C*, *d*) lacks the pronounced peak seen in the corresponding component of α_{1C} cells (Fig. 7 *B*, *d*). In addition, the

FIGURE 9 Ca^{2+} mobilization from extra- and intracellular sources by voltage-dependent Ca^{2+} channels of different properties. The scheme summarizes the interpretation of experimental data obtained in this study. (A) The skeletal muscle-type α_{1S} responds to depolarization with an intramolecular charge movement that initiates direct conformational coupling to the RyR1 causing voltage-dependent Ca^{2+} release (*VDCR*). This leads to a primary Ca^{2+} signal in the junctional gap. The small and slow Ca^{2+} inward current plays a negligible role in Ca^{2+} mobilization and is omitted in the scheme. The released Ca^{2+} enhances further Ca^{2+} release leading to a secondary Ca^{2+}-induced Ca^{2+} release flux component (*CICR*) that has phasic and tonic components. VDCR and CICR together make up the Ca^{2+} input flux. (B) The cardiac muscle-type DHPR likewise responds to depolarization with an intramolecular charge movement that also results in a primary Ca^{2+} signal but by voltage-induced Ca^{2+} inward current (Ca^{2+} entry) instead of VDCR. This also leads to CICR, which, together with the Ca^{2+} entry flux, makes up total Ca^{2+} input flux. (C) The brain α_{1A}-subunit, which is not positioned close to the ryanodine receptors, generates a rapid global Ca^{2+} entry flux signal, although probably a much slower and smaller primary junctional Ca^{2+} signal than α_{1S} or α_{1C}, leading to ineffective CICR (lacking the phasic component). α_{1}Aas(1592-clip) shows a phasic component unlike α_{1A} but not as large as in α_{1S} or α_{1C}, probably because not enough α_{1}Aas(1592-clip) subunits become positioned close to the RyRs. See Discussion for further explanations.

voltage-dependence of the Ca^{2+} signals in α_{1C} cells was different. It was shifted to more negative potentials, with respect to the voltage-dependence of Ca^{2+} inward current activation (Fig. 4 *B*). This is a characteristic also found in heart cells and has been attributed to the stronger driving force for Ca^{2+} entry at more negative potentials leading to a higher gain of Ca^{2+}-induced-Ca^{2+} release (Wier et al., 1994). It is a consequence of the local control of Ca^{2+}-induced Ca^{2+} release that depends on local single-channel currents rather than on global Ca^{2+}-current amplitudes (Cheng and Wang, 2002). In contrast, in α_{1A}-expressing cells the voltage-dependence of Ca^{2+} signal and Ca^{2+} current was more similar (Figs. 3 and 4 *C*). These results point to the presence of a more efficient Ca^{2+}-induced Ca^{2+}-release component in α_{1C}-expressing cells compared to α_{1A}-expressing cells.

Because the transient CPA- and caffeine-sensitive flux component present in α_{1C} but not in α_{1A} cells occurs at the beginning of the depolarizing voltage step, it may be responsible for the much more frequent appearance of Ca^{2+} signals upon short extracellular stimuli in α_{1C}-expressing myotubes (Flucher et al., 2000). As suggested by Flucher et al. (2000), a plausible reason is the specific targeting of α_{1C} to the sarcolemma-SR junctions. Another possibility for the lower responsiveness of α_{1A}-expressing myotubes would be a higher failure rate to elicit all-or-none action potentials,

even though it is difficult to see how such a failure would come about.

Gain determinations

The amplification process in Ca^{2+}-induced Ca^{2+} release has been studied in detail in cardiac myocytes and is usually quantified by calculating an EC coupling gain factor (for review, see Bers, 2001). Previous determinations of global gain derived from whole-cell measurements in heart cells were based on estimates of integral (total) Ca^{2+} (e.g., Shannon et al., 2000) or of the corresponding Ca^{2+} fluxes (e.g., Wier et al., 1994). The latter approach was also used in the present study and allowed a quantitative comparison of Ca^{2+} entry flux and total Ca^{2+} input flux to the myoplasm.

As a second approach to estimating amplification by Ca^{2+} release, we compared the change in intracellular Ca^{2+} caused by identical trigger pulses before and after depleting the SR of its stored Ca^{2+}. In our experiments, the Ca^{2+} input flux controlled by the α_{1S}-subunit was almost completely suppressed by the depletion procedure, demonstrating that it originated almost exclusively from SR Ca^{2+} release. In the presence of the other Ca_V channels tested, the Ca^{2+} current itself made a relatively large contribution to the total Ca^{2+} input flux, but not even in the case of α_{1A} was secondary Ca^{2+} release completely absent.

Our experiments indicated a lower gain in α_{1C}-transfected GLT cells (+30 mV) than in mature heart cells, for which values close to 10 have been estimated in a voltage range of comparable fractional activation (Wier et al., 1994). Reasons might be a higher coupling fidelity of RyR2 in cardiac myocytes compared to RyR1 in skeletal myotubes or a steeper Ca^{2+} gradient produced by the SERCA pump. In heart cells, gain was shown to exhibit a strong dependence on the concentration of Ca^{2+} in the SR lumen (Shannon et al., 2000). In the myotubes, a rather low rate of uptake, likely associated with establishing a smaller gradient, is indicated by the slow change of the signal at the end of a depolarization, which has been observed by us and others (García and Beam, 1994). However, strong differences in SR loading between the four constructs tested is unlikely, since a similar response on application of CPA/caffeine could be observed (see Fig. 6 *B*).

α_1Aas(1592-clip) characteristics

Surprisingly, α_1Aas(1592-clip)-expressing cells did not show a fundamentally different pattern than α_{1A}-type cells despite the observed differences in junctional targeting. Both Ca^{2+} inward current and Ca^{2+} input flux were larger than for α_{1A}, but regarding gain they can at best be described as intermediate between α_{1A} and α_{1C} cells. The smaller gain at larger current density is reminiscent of the situation in heart cells where β-adrenergic up-regulation of Ca^{2+} inward current does not increase the Ca^{2+} signal proportionally (Song et al., 2001). A fast CPA/caffeine-sensitive component was detectable in α_1Aas(1592-clip) (Fig. 7 *D, d*), but its amplitude was smaller than in α_{1C}. Also, the voltage-dependence of Ca^{2+} inward current and Ca^{2+} signal (Figs. 3 and 4) resembled more α_{1A} than α_{1C}. The significantly larger Ca^{2+} input flux in α_1Aas(1592-clip) compared to α_{1A} resulted mainly from the larger Ca^{2+} entry flux, not from an increase in gain.

From the present and previous results it seems that the C-terminal signal sequence of the L-type channel introduced into α_1Aas(1592-clip) improves the level of expression but may not establish full α_{1C}-type Ca^{2+}-induced Ca^{2+} release despite the junctional targeting. In dual immunostaining experiments for the localization of α_1-subunits and RyRs, a cell is labeled *colocalized* if regions of colocalization are detectable (Flucher et al., 2000). This criterion makes a quantitative comparison with electrophysiological measurements difficult, because an uncertain percentage of the Ca$_V$ channels that participate in the functional signals may not be colocalized with RyR1. Moreover, the density of channels in the junction, a crucial determinant for establishing efficient cardiac type EC coupling, may well be considerably smaller in α_1Aas(1592-clip)-expressing cells than in α_{1C} cells. The global Ca^{2+} current density was comparable, but the open probability of α_{1A} in dysgenic myotubes is thought to be higher than that of α_{1C}. This

follows from the much larger whole-cell current measured per voltage-sensor charge movements (Adams et al., 1994). Longer openings provide more local Ca^{2+} per channel. However, it appears to be the amount of Ca^{2+} supplied immediately on opening of a Ca$_V$1.2 channel that triggers Ca^{2+} release (Song et al., 2001). Therefore, longer openings are not necessarily more effective than short openings and are unlikely to compensate for a lower channel density in the junction. Ca^{2+} channels that are not specifically targeted, such as the α_{1A} channels, may generate a slowly rising junctional Ca^{2+} transient from diffusional delays, which may still cause a secondary efflux of Ca^{2+} from the SR (CICR in Fig. 7 *C*). However, this release is less synchronized, explaining the different shape of the CPA/caffeine-sensitive component in Fig. 7 C (*d*), which lacks a peak. α_1Aas(1592-clip) which is targeted to the junction may not reach a sufficient density there to provide the same local trigger flux of Ca^{2+} as α_{1C}. This may be the reason why cells expressing this isoform show a behavior intermediate between Fig. 9, *B* and *C*.

CONCLUSION

In summary, we compared, in the same cellular expression system, properties of interaction of different Ca$_V$ channel α_1-subunits with the ryanodine receptor RyR1. The observations made here in voltage-clamped myotubes helped us to reconcile previous results from immunocytochemical localization studies and measurements of action-potential stimulated Ca^{2+} transients. In these studies, introducing the putative junctional targeting sequence into α_{1A} had been shown to increase the response frequency approximately ninefold, but not nearly to the level of α_{1C}-expressing cells (140-fold; see Flucher et al., 2000). We conclude that these differences result from different junctional channel densities and single-channel gating properties leading to characteristic local Ca^{2+} signals near the RyRs. To investigate the local functional properties of Ca^{2+} signaling of heterologously expressed channels in further detail will require more refined methods. A promising recent approach has been the recording of Ca^{2+} currents, i.e., *sparklets* and *sparks* from small junctional regions of patch-clamped cardiac myocytes (Wang et al., 2001).

REFERENCES

Adams, B. A., Y. Mori, M. S. Kim, T. Tanabe, and K. G. Beam. 1994. Heterologous expression of BI Ca^{2+} channels in dysgenic skeletal muscle. *J. Gen. Physiol.* 104:985–996.

Ahern, C. A., D. Bhattacharya, L. Mortenson, and R. Coronado. 2001. A component of excitation-contraction coupling triggered in the absence of the T671–L690 and L720–Q765 regions of the II–III loop of the dihydropyridine receptor α_{1S} pore subunit. *Biophys. J.* 81:3294–3307.

Baylor, S. M., W. K. Chandler, and M. W. Marshall. 1983. Sarcoplasmic reticulum calcium release in frog skeletal muscle fibres estimated from Arsenazo III calcium transients. *J. Physiol.* 344:625–666.

Baylor, S. M., and S. Hollingworth. 1998. Model of sarcomeric Ca^{2+} movements, including ATP Ca^{2+} binding and diffusion, during activation of frog skeletal muscle. *J. Gen. Physiol.* 112:297–316.

Beam, K. G., and P. Horrowitz. 2004. Excitation-contraction coupling in skeletal muscle. *In* Myology. C. Franzini-Armstrong, and A.G. Engel, editors. McGraw-Hill, New York. 257–280.

Bers, D. M. 2001. Excitation-Contraction Coupling and Cardiac Contractile Force. Kluwer Academic Publishers, Dordrecht, the Netherlands.

Beurg, M., C. A. Ahern, P. Vallejo, M. W. Conklin, P. A. Powers, R. G. Gregg, and R. Coronado. 1999a. Involvement of the carboxy-terminus region of the dihydropyridine receptor β_{1A} subunit in excitation-contraction coupling of skeletal muscle. *Biophys. J.* 77:2953–2967.

Beurg, M., M. Sukhareva, C. A. Ahern, M. W. Conklin, E. Perez-Reyes, P. A. Powers, R. G. Gregg, and R. Coronado. 1999b. Differential regulation of skeletal muscle L-type Ca^{2+} current and excitation-contraction coupling by the dihydropyridine receptor β-subunit. *Biophys. J.* 76:1744–1756.

Cheng, H., and S. Q. Wang. 2002. Calcium signaling between sarcolemmal calcium channels and ryanodine receptors in heart cells. *Front. Biosci.* 7:d1867–d1878.

Csernoch, L., V. Jacquemond, and M. F. Schneider. 1993. Microinjection of strong calcium buffers suppresses the peak of calcium release during depolarization in frog skeletal muscle fibers. *J. Gen. Physiol.* 101:297–333.

Csernoch, L., P. Szentesi, and L. Kovacs. 1999a. Differential effects of caffeine and perchlorate on excitation-contraction coupling in mammalian skeletal muscle. *J. Physiol.* 520:217–230.

Csernoch, L., P. Szentesi, S. Sarkozi, C. Szegedi, I. Jona, and L. Kovacs. 1999b. Effects of tetracaine on sarcoplasmic calcium release in mammalian skeletal muscle fibres. *J. Physiol.* 515:843–857.

Delbono, O., and E. Stefani. 1993. Calcium transients in single mammalian skeletal muscle fibres. *J. Physiol.* 463:689–707.

DelPrincipe, F., M. Egger, and E. Niggli. 1999. Calcium signalling in cardiac muscle: refractoriness revealed by coherent activation. *Nat. Cell Biol.* 1:323–329.

Dietze, B., F. Bertocchini, V. Barone, A. Struk, V. Sorrentino, and W. Melzer. 1998. Voltage-controlled Ca^{2+} release in normal and ryanodine receptor type 3 (RyR3)-deficient mouse myotubes. *J. Physiol.* 513:3–9.

Dietze, B., J. Henke, H. M. Eichinger, F. Lehmann-Horn, and W. Melzer. 2000. Malignant hyperthermia mutation $Arg^{615}Cys$ in the porcine ryanodine receptor alters voltage dependence of Ca^{2+} release. *J. Physiol.* 526:507–514.

Dirksen, R. T. 2002. Bi-directional coupling between dihydropyridine receptors and ryanodine receptors. *Front. Biosci.* 7:d659–d670.

Flucher, B. E., N. Kasielke, and M. Grabner. 2000. The triad targeting signal of the skeletal muscle calcium channel is localized in the COOH terminus of the α_{1S} subunit. *J. Cell Biol.* 151:467–478.

Föhr, K. J., W. Warchol, and M. Gratzl. 1993. Calculation and control of free divalent cations in solutions used for membrane fusion studies. *Methods Enzymol.* 221:149–157.

Franzini-Armstrong, C. 2004. The Membrane Systems of Muscle Cells. *In* Myology. C. Franzini-Armstrong, and A.G. Engel, editors. McGraw-Hill, New York. 232–256.

Franzini-Armstrong, C., F. Protasi, and V. Ramesh. 1998. Comparative ultrastructure of Ca^{2+} release units in skeletal and cardiac muscle. *Ann. N. Y. Acad. Sci.* 853:20–30.

Franzini-Armstrong, C., F. Protasi, and V. Ramesh. 1999. Shape, size, and distribution of Ca^{2+} release units and couplons in skeletal and cardiac muscles. *Biophys. J.* 77:1528–1539.

García, J., and K. G. Beam. 1994. Measurement of calcium transients and slow calcium current in myotubes. *J. Gen. Physiol.* 103:107–123.

García, J., and M. F. Schneider. 1993. Calcium transients and calcium release in rat fast-twitch skeletal muscle fibres. *J. Physiol.* 463:709–728.

García, J., T. Tanabe, and K. G. Beam. 1994. Relationship of calcium transients to calcium currents and charge movements in myotubes expressing skeletal and cardiac dihydropyridine receptors. *J. Gen. Physiol.* 103:125–147.

Grabner, M., R. T. Dirksen, and K. G. Beam. 1998. Tagging with green fluorescent protein reveals a distinct subcellular distribution of L-type and non-L-type Ca^{2+} channels expressed in dysgenic myotubes. *Proc. Natl. Acad. Sci. USA.* 95:1903–1908.

Grabner, M., R. T. Dirksen, N. Suda, and K. G. Beam. 1999. The II–III loop of the skeletal muscle dihydropyridine receptor is responsible for the bi-directional coupling with the ryanodine receptor. *J. Biol. Chem.* 274:21913–21919.

Herrmann-Frank, A., H. C. Lüttgau, and D. G. Stephenson. 1999. Caffeine and excitation-contraction coupling in skeletal muscle: a stimulating story. *J. Muscle Res. Cell Motil.* 20:223–237.

Jurkat-Rott, K., U. Uetz, U. Pika-Hartlaub, J. Powell, B. Fontaine, W. Melzer, and F. Lehmann-Horn. 1998. Calcium currents and transients of native and heterologously expressed mutant skeletal muscle DHP receptor $\alpha1$ subunits (R528H). *FEBS Lett.* 423:198–204.

Klein, M. G., B. J. Simon, G. Szücs, and M. F. Schneider. 1988. Simultaneous recording of calcium transients in skeletal muscle using high- and low-affinity calcium indicators. *Biophys. J.* 53:971–988.

Leberer, E., and D. Pette. 1986. Neural regulation of parvalbumin expression in mammalian skeletal muscle. *Biochem. J.* 235:67–73.

Melzer, W., A. Herrmann-Frank, and H. C. Lüttgau. 1995. The role of Ca^{2+} ions in excitation-contraction coupling of skeletal muscle fibres. *Biochim. Biophys. Acta.* 1241:59–116.

Melzer, W., E. Rios, and M. F. Schneider. 1984. Time course of calcium release and removal in skeletal muscle fibers. *Biophys. J.* 45:637–641.

Nakai, J., T. Tanabe, T. Konno, B. Adams, and K. G. Beam. 1998. Localization in the II–III loop of the dihydropyridine receptor of a sequence critical for excitation-contraction coupling. *J. Biol. Chem.* 273:24983–24986.

Powell, J. A., L. Petherbridge, and B. E. Flucher. 1996. Formation of triads without the dihydropyridine receptor α-subunits in cell lines from dysgenic skeletal muscle. *J. Cell Biol.* 134:375–387.

Proenza, C., C. Wilkens, N. M. Lorenzon, and K. G. Beam. 2000. A carboxyl-terminal region important for the expression and targeting of the skeletal muscle dihydropyridine receptor. *J. Biol. Chem.* 275:23169–23174.

Rüegg, J. C. 1986. Calcium in Muscle Activation. Springer, Berlin, Heidelberg, New York.

Schuhmeier, R. P., B. Dietze, D. Ursu, F. Lehmann-Horn, and W. Melzer. 2003. Voltage-activated calcium signals in myotubes loaded with high concentrations of EGTA. *Biophys. J.* 84:1065–1078.

Schuhmeier, R. P., and W. Melzer. 2004. Voltage-dependent Ca^{2+} fluxes in skeletal myotubes determined using a removal model analysis. *J. Gen. Physiol.* 123:33–51.

Shannon, T. R., K. S. Ginsburg, and D. M. Bers. 2000. Potentiation of fractional sarcoplasmic reticulum calcium release by total and free intra-sarcoplasmic reticulum calcium concentration. *Biophys. J.* 78:334–343.

Shirokova, N., J. García, G. Pizarro, and E. Ríos. 1996. Ca^{2+} release from the sarcoplasmic reticulum compared in amphibian and mammalian skeletal muscle. *J. Gen. Physiol.* 107:1–18.

Song, L. S., S. Q. Wang, R. P. Xiao, H. Spurgeon, E. G. Lakatta, and H. Cheng. 2001. β-Adrenergic stimulation synchronizes intracellular

Ca^{2+} release during excitation-contraction coupling in cardiac myocytes. *Circ. Res.* 88:794–801.

Ursu, D., R. P. Schuhmeier, M. Freichel, V. Flockerzi, and W. Melzer. 2004. Altered inactivation of Ca^{2+} current and Ca^{2+} release in mouse muscle fibers deficient in the DHP receptor γ1 subunit. *J. Gen. Physiol.* 124:605–618.

Ursu, D., S. Sebille, B. Dietze, D. Freise, V. Flockerzi, and W. Melzer. 2001. Excitation-contraction coupling in skeletal muscle of a mouse lacking the dihydropyridine receptor subunit γ$_1$. *J. Physiol.* 533:367–377.

Wang, S. Q., L. S. Song, E. G. Lakatta, and H. Cheng. 2001. Ca^{2+} signalling between single L-type Ca^{2+} channels and ryanodine receptors in heart cells. *Nature.* 410:592–596.

Wier, W. G., T. M. Egan, J. R. Lopez-Lopez, and C. W. Balke. 1994. Local control of excitation-contraction coupling in rat heart cells. *J. Physiol.* 474:463–471.